Chapter 13

Raman Scattering Study on the Phase Transition Dynamics of Ferroelectric Oxides

Hiroki Taniguchi, Hiroki Moriwake, Toshirou Yagi and Mitsuru Itoh

Additional information is available at the end of the chapter

http://dx.doi.org/10.5772/52059

1. Introduction

Ferroelectric phase transitions are conventionally divided into two types: an order-disorder and a displacive-type.[1] In the former one, which is frequently seen in hydrogen-bond-type ferroelectrics such as KH_2PO_4 (KDP), local dipole moments μs are randomly distributed between opposite directions in the paraelectric phase, leading to zero macroscopic net polarization P (= $\Sigma\mu$). A spontaneous polarization in the ferroelectric phase is then driven by their ordering through the ferroelectric phase transition. In the later type, in contrast, there are no dipole moments in the paraelectric phase. The spontaneous polarization in the ferroelectric phase stems from relative polar displacement between cationic and anionic sublattices. It is induced by freezing of a so-called ferroelectric "soft mode", which is known as a strongly anharmonic optical phonon mode at Γ-point in the Brillouin zone (BZ). The displacive-type transition is often found in the ferroelectric oxides as represented by perovskite-type compounds such as $PbTiO_3$. Since the ferroelectric oxides have been widely applied for the electronic devices, such as actuators, sensors, and memories, due to their chemical stability, the large spontaneous polarization, and the relatively high transition temperature, a better understanding of the soft mode behavior would be important from viewpoints of both application and fundamental sciences. Spectroscopic techniques employing light scattering, infrared absorption, and neutron scattering have been generally utilized for investigating the dynamics of the soft mode. Among them, Raman scattering has an advantage especially in a low-frequency region, which is significant to resolve the critical dynamics of the soft mode near the transition temperature. In the present review, we will discuss the soft mode behavior at the ferroelectric phase transition by referring the Raman scattering studies on $CdTiO_3$ and ^{18}O-substituted $SrTiO_3$. Furthermore, a microscopic origin of the soft mode is figured out from a viewpoint of local chemical bonds with the help of first-principles calculations.

2. Ferroelectric soft mode in the classical scheme

Since a concept of the soft mode was proposed, many theoretical and experimental studies have been conducted to clarify its dynamics.[2-4] In this section, we discuss the soft mode behavior in the classical scheme.

2.1. Theoretical background of the ferroelectric soft mode in the classical scheme

The potential of the soft mode is approximately described by accounting only a biquadratic phonon-phonon interaction as follows:

$$U_0 = \frac{1}{2}M(s,0)\omega_{\text{bare}}^2(s,0)Q^2(s,0) + \sum_{\lambda}\sum_{k}\frac{1}{2}J(s,0;\lambda,k)Q^2(s,0)Q^2(\lambda,k) \tag{1}$$

where $M(s,0)$, $\omega_{\text{bare}}(s,0)$, $Q(s,0)$ in the first term are effective mass, bare frequency, and displacement of the soft mode at the Γ-point. The $J(s,0;\lambda,k)$ in the second term denotes an interaction between the soft mode at the Γ-point and the optical phonon mode λ at the wave vector k, where the summation runs over all blanches and BZ. The equation can be transformed by a pseudo-harmonic approximation as

$$\begin{aligned} U_0 &\approx \frac{1}{2}M(s,0)\omega_{\text{bare}}^2(s,0)Q^2(s,0) + \sum_{\lambda}\sum_{k}\frac{1}{2}J(s,0;\lambda,k)Q^2(s,0)\left\langle Q^2(\lambda,k)\right\rangle \\ &= \frac{1}{2}M(s,0)\left[\omega_{\text{bare}}^2(s,0) + \sum_{\lambda}\sum_{k}\frac{J(s,0;\lambda,k)}{M(s,0)}\left\langle Q^2(\lambda,k)\right\rangle\right]Q^2(s,0) \\ &\equiv \frac{1}{2}M(s,0)\omega_{\text{s}}^2Q^2(s,0) \end{aligned} \tag{2}$$

where the inside of the brackets is redefined by the soft mode frequency ω_s. In the classical regime, the mean square displacement $\langle Q^2(\lambda,k)\rangle$ is proportional to k_BT, where k_B is a Boltzmann constant. The soft mode frequency is thus expressed as

$$\omega_{\text{s}}^2 \equiv \omega^2(s,0) = \omega_{\text{bare}}^2(s,0) + \sum_{\lambda}\sum_{k}\frac{J(s,0;\lambda,k)}{M(s,0)}\frac{k_{\text{B}}T}{M(\lambda,k)\omega^2(\lambda,k)} \tag{3}$$

Since ω_s is ideally zero at T_c of the second-order phase transition,

$$\omega_{\text{s}}^2 = \omega_{\text{bare}}^2(s,0) + \sum_{\lambda}\sum_{k}\frac{J(s,0;\lambda,k)}{M(s,0)}\frac{k_{\text{B}}T_{\text{c}}}{M(\lambda,k)\omega^2(\lambda,k)} = 0 \tag{4}$$

leading to

$$\omega_{\text{bare}}^2(s,0) = -\sum_{\lambda}\sum_{k}\frac{J(s,0;\lambda,k)}{M(s,0)}\frac{k_{\text{B}}T_{\text{c}}}{M(\lambda,k)\omega^2(\lambda,k)} \tag{5}$$

We thus obtain

$$\omega_{\text{s}}^2 = \sum_{\lambda}\sum_{k}\frac{J(s,0;\lambda,k)}{M(s,0)}\frac{k_{\text{B}}T}{M(\lambda,k)\omega^2(\lambda,k)} - \sum_{\lambda}\sum_{k}\frac{J(s,0;\lambda,k)}{M(s,0)}\frac{k_{\text{B}}T_{\text{c}}}{M(\lambda,k)\omega^2(\lambda,k)} \tag{6}$$

Defining C as

$$C \equiv \left[\sum_{\lambda}\sum_{k}\frac{J(s,0;\lambda,k)}{M(s,0)}\frac{k_{\text{B}}}{M(\lambda,k)\omega^2(\lambda,k)}\right]^{1/2} \tag{7}$$

it finally comes to Cochran's law

$$\omega_{\text{s}} = C(T - T_{\text{c}})^{1/2} \tag{8}$$

where

$$T_{\text{c}} \equiv -\omega_{\text{bare}}^2(s,0)\left[\sum_{\lambda}\sum_{k}\frac{J(s,0;\lambda,k)}{M(s,0)}\frac{k_{\text{B}}}{M(\lambda,k)\omega^2(\lambda,k)}\right]^{-1} \tag{9}$$

As seen in the above equation, the soft mode decreases its frequency with approaching T_c, and finally freezes to induce the ferroelectric phase transition. In the second-order phase transition, in particular, the displacement of the soft mode $Q(s,0)$ corresponds to the polar displacement in the ferroelectric phase. It should be noted that the bare frequency $\omega_{\text{bare}}(s,0)$ of the soft mode is assumed to be imaginary at zero-Kelvin. The softening of the soft mode connects to the divergent increase of the dielectric constant through Lyddane-Sachs-Teller (LST) relation,

$$\varepsilon' \propto \frac{1}{\omega_{\text{s}}^2} \tag{10}$$

2.2. Experimental observation of the ferroelectric soft mode in the classical scheme

The experimental observation of the typical soft mode behavior in the perovskite-type ferroelectric oxide, $CdTiO_3$, is presented in this section.

$CdTiO_3$ possesses an orthorhombic *Pnma* structure at room temperature due to ($a^+b^-b^-$)-type octahedral rotations in the Glazer's notation from the prototypical Cubic *Pm*-3*m* structure. The $CdTiO_3$ undergoes ferroelectric phase transition into the orthorhombic $Pna2_1$ phase around 85 K.[5-7]

The confocal micro-Raman scattering is the one of useful techniques to investigate the soft mode dynamics in the displacive-type ferroelectric phase transition due to the following reason; In general, the complicated domain structure forms across the ferroelectric phase transition, where the principle axis of the crystal orients to various directions, which are allowed by the symmetry relation between the paraelectric and the ferroelectric phases. The size of the individual domain generally ranges over several nanometers to microns. When the domains are smaller than the radiated area of the incident laser, the observed Raman spectrum is composed of signals from differently oriented domains, leading to difficulty in the precise spectral analyses. With application of the confocal micro-Raman scattering, on the other hand, we can selectively observe the spectrum from the single domain region, because its spatial resolution reaches sub-microns not only for lateral but also depth directions.[8] Note that the Raman scattering can observe the soft mode only in the non-centrosymmetric phase due to the selection rule, therefore the critical dynamics of the soft mode is in principle investigated in the ferroelectric phase below T_c.

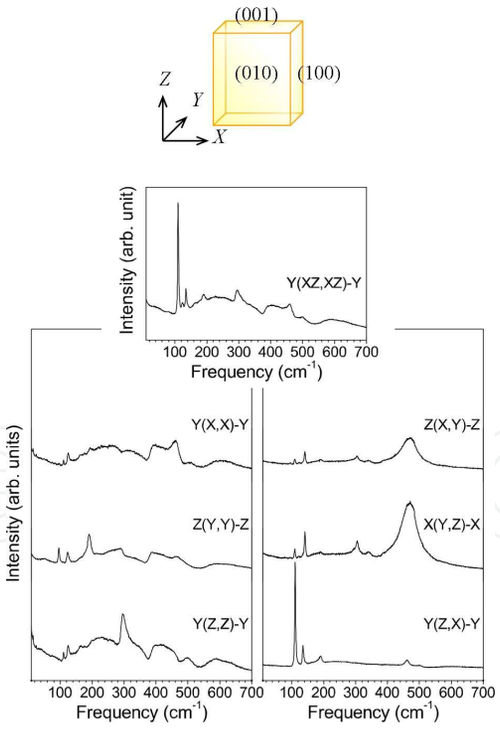

Figure 1. Raman spectra of $CdTiO_3$ at room temperature observed with several scattering geometries. See text for configuration notations, for instance Y(X,X)-Y.

Flux-grown colorless single crystals of $CdTiO_3$ with a rectangular solid shape were used for this study. The two samples have dimensions of approximately 0.3×0.2×0.1 mm^3 and

http://dx.doi.org/10.5772/52059

0.2×0.1×0.1 mm^3. Since the present samples were twinned, we carefully determined the directions of the axes in the observed area by checking the angular dependence of the Raman spectra with the confocal micro-Raman system, whose spatial resolution is around 1 μm (Fig. 1). Here we use laboratory coordinates X, Y, and Z, corresponding respectively to the crystallographic axes of [100], [010], and [001] in the paraelectric phase, to denote the Raman scattering geometries. For example, XZ(Y,Y)-Z-X means that the incident laser polarized parallel to the [010] direction penetrates the sample along the [101] direction, and the [010]-polarized scattered light is collected with the backscattering geometry. The scattered light was analyzed by a Jovin-Yvon triple monochromator T64000 with the subtractive dispersion mode, and was finally observed by a liquid-N_2-cooled CCD camera. The frequency resolution of the present experiment was better than 1 cm^{-1} The temperature of the sample was controlled by an Oxford microstat with a temperature stability of ±0.01 K.

Figure 2 shows the temperature dependence of the Raman spectrum of $CdTiO_3$, which is observed in Y(ZX,ZX)-Y scattering geometry with several temperatures from 85.0 K to 40.0 K. In the vicinity of T_c, in particular, spectra were observed with the temperature intervals of 0.5 K. As shown in the figures, the soft mode is seen at around 60 cm^{-1} at 40 K. It gradually softens toward zero-frxuency as approaching T_c ~ 85 K. The spectral profile of the soft mode is analyzed by a damped-harmonic-oscillator (DHO) model;

$$I(\omega) = \frac{B\omega_0^2 \Gamma \omega}{(\omega_0^2 - \omega^2)^2 + \Gamma^2 \omega^2} \tag{11}$$

where B, ω_0, and Γ denote amplitude, harmonic frequency, and a damping constant of the soft mode, respectively. The soft mode frequency ω_s is defined here as

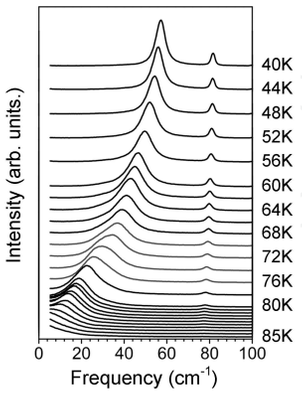

Figure 2. Temperature Dependence of the Raman spectrum of $CdTiO_3$ observed in the Y(ZX,ZX)-Y scattering geometry, and from 40K to 85 K on heating.

$$\omega_s^2 = \sqrt{\omega_0^2 - \Gamma^2} \tag{12}$$

The temperature dependence of the soft mode frequency and the damping constant, which are determined by the analyses, are plotted by solid circles and open squares in Fig. 3. Synchronizing with the softening of the soft mode, the damping constant is increased as approaching T_c.

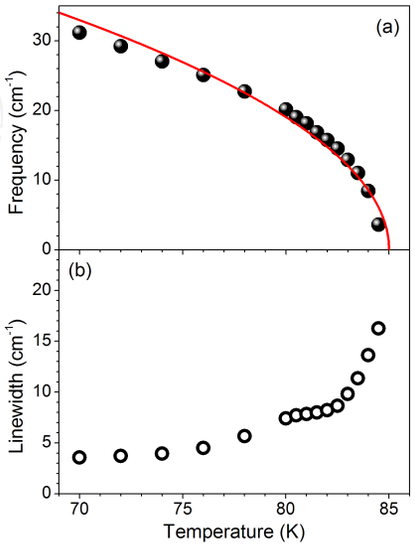

Figure 3. Temperature Dependencies of (a) the soft mode frequency and (b) the damping constant of $CdTiO_3$. The solid line in (a) is calculated by Cochran's law (see text).

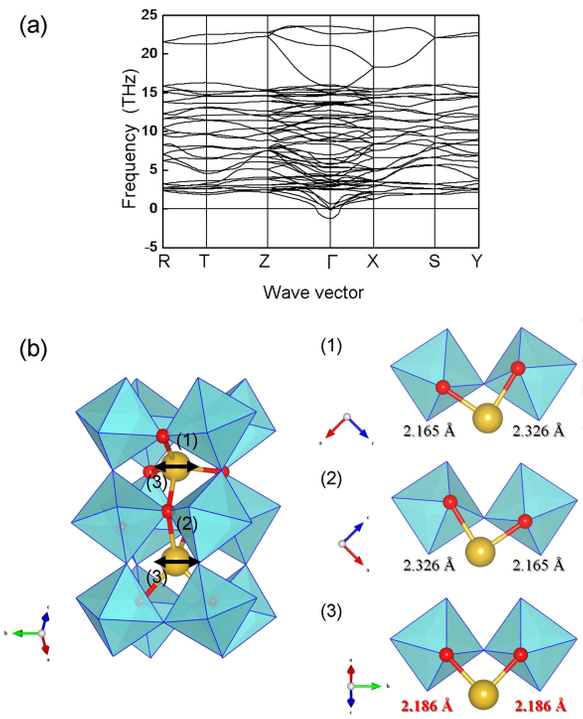

Figure 4. a) Phonon dispersion in $CdTiO_3$ obtained by the first-principles calculations. (b) The displacement pattern of the soft mode, and configurations of three O-Cd-O bonds along (1) [-101], (2) [101], and (3) [010] directions.

The temperature dependence of the soft mode frequency obeys the Cochran's low (Eq. 1.8) with $C = 8.5$ and $T_c = 85$ K as expressed by the solid curve in the figure, indicating the typical displacive-type ferroelectric phase transition on $CdTiO_3$.

The displacement pattern of the soft mode is obtained by first principle calculations. The calculations were conducted with a pseudopotential method based on a density functional perturbation theory with norm-conserving pseudopotentials, which was implemented in the CASTEP code.[9] Figure 4a presents phonon dispersion curves of $CdTiO_3$ in the paraelectric *Pnma* phase, which was obtained by the first-principle calculations. As seen in the figure, the soft mode, which is indicated by an imaginary frequency, is observed at Γ-point in Brillouin zone. According to the calculation, a displacement pattern of the Γ-point soft mode is composed of relative displacement of Ti with respective to the octahedra and an asymmetric stretching of O-Cd-O bond. It has been previously proposed that the hybridization between O-2p and empty Ti-3d orbitals triggers the non-centrosymmetric displacement of Ti thorough a second-order Jahn-Teller (SOJT) effect to induce the ferroelectricity as exemplified by $BaTiO_3$.[10] The SOJT effect, however, does not provide clear understanding on the role of *A*-site ion. In the case of $CdTiO_3$, in particular, the ferroelectricity disappears when the Cd is replaced by Ca, though the $CaTiO_3$ is an isomorph of $CdTiO_3$. Therefore, the ferroelectricity in $CdTiO_3$ can not be explained only by the *B*-O orbital hybridization. Here, we focus on the asymmetric stretching of O-Cd-O to elucidate the mechanism of ferroelectricity in $CdTiO_3$. The asymmetric stretching in the Γ-point soft mode is schematically illustrated by arrows in the right panel in Fig. 4b, where large and small spheres denote Cd and O ions, respectively. Ti and O ions that do not participate in the O-Cd-O bonds are omitted for simplicity. In a prototypical *Pm*-3*m* structure of the perovskite-type oxide, an *A*-site ion is surrounded by neighboring twelve O ions. In the $CdTiO_3$ of paraelectric *Pnma* structure, however, the number of closest oxygen ions for Cd ion is reduced to four due to the octahedral rotations. (Note that the octahedral rotations in the *Pnma* structure are different from each other according to the direction; the rotation is in-phase for a [010] direction whereas those for [101] and [-101] are anti-phase.) As a result, $CdTiO_3$ has three different O-Cd-O bonds along [-101], [101], and [010] directions, whose equilibrium structures are respectively denoted by (1), (2), and (3) in the Fig. 2(b). The result of first-principles calculations indicates that the soft mode displacement is inherently dominated by the asymmetric stretching of the O-Cd-O bond along the [010] direction denoted by (3). By comparing three equilibrium structures for O-Cd-O bonds presented in the right-hand side of Fig. 4b, it is found that the O-Cd-O bond along [010] direction is symmetric with the Cd-O bond lengths of 2.186 Å in the paraelectric *Pnma* phase, in contrast the other two are composed of non-equivalent bonds having 2.326 and 2.165 Å. Therefore, there is a remaining degree of freedom for further O-Cd-O off-center ordering due to the covalent bonding along the [010] direction. This remaining degree of freedom would be the origin of the ferroelectric soft mode.

3. A role of covalency in the ferroelectric soft mode

As indicated above, the covalency of the *A*-site ion plays an important role in the ferroelectricity in addition to that of *B*-site ion. The *A*-site substitution with an isovalent ion is in-

structive for the better understanding on the mechanism of the ferroelectricity in the perovskite-type oxides. This section is thus devoted to the effect of the isovalent Ca-substitution on the ferroelectricity of $CdTiO_3$. [11, 12]

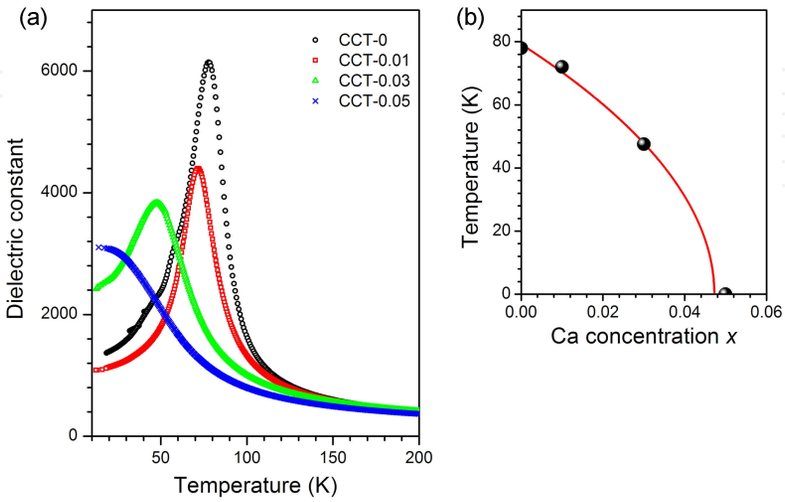

Figure 5. a) Dielectric constants of CCT-*x*. (b) Ca concentration dependence of the ferroelectric phase transition temperature T_c. Solid curve denotes Curie–Weiss fit of data points for CCT-0, 0.01, and 0.03.

Ceramics form of Ca-doped $CdTiO_3$, $Cd_{1-x}Ca_xTiO_3$ (CCT-*x*) with x = 0, 0.01, 0.03, 0.05, and 0.07, were fabricated by conventional solid state reactions from stoichiometric mixtures of CdO (3N), $CaCO_3$ (4N), and TiO_2 (3N). The mixtures were calcined during 24 h in air at 975 ~ 1175ºC. Then the reground powders were pressed at 4 ton/cm^2, and sintered at 1200 ~ 1230ºC. Dielectric measurements were performed by a LCZ meter.

Temperature dependencies of the dielectric constants in CCT-*x* are presented in Fig. 5a. As seen in the figure, the dielectric constant of CCT-0 divergently increases and culminates at the phase transition temperature T_c ~ 85 K. The T_c decreases with Ca doping, and the peak transforms into a low-temperature plateau at x = 0.05, indicating a quantum paraelectric state as discussed later. The Ca concentration dependence of T_c, which is estimated from the dielectric peaks, is shown in Fig. 5b. The fit curve with conventional Curie-Weiss law (a red line in the figure) indicates that the ferroelectricity in the CCT-*x* system is suppressed with a value of x larger than x_c = 0.047.

The temperature dependence of the soft mode frequency is presented in Fig. 6 as a function of x. The soft modes in CCT-*x* increase in frequency and intensity with distance from T_c on cooling, exhibiting typical behavior of the soft-mode-driven phase transition. According to the Lyddane–Sachs–Teller relationship (Eq. 1.10), the squared soft mode frequency ω_s^2 and the dielectric constant ε' are inversely proportional as mentioned in the preceding section. Therefore, if the dielectric properties of the CCT-*x* system are governed by the lattice dynamics, the soft mode frequency at the lowest temperature should de-

http://dx.doi.org/10.5772/52059

crease with increasing x because the dielectric constant near 0 K increases with x (see Fig. 5a). The Raman spectra at 4 K presented in the bottom panels in Fig. 6 show that the soft mode softens as x increases, indicating a displacive-type phase transition of the CCT-x system. This result suggests that the phase transition of CCT-x can be discussed in terms of lattice dynamics. Note that, the soft mode become observable at low temperature in CCT-0.05 and -0.07, although it does not undergo the ferroelectric phase transition within a finite temperature range. This is a typical characteristic of precursory softening of the soft mode in the quantum paraelectric state.[13, 14]

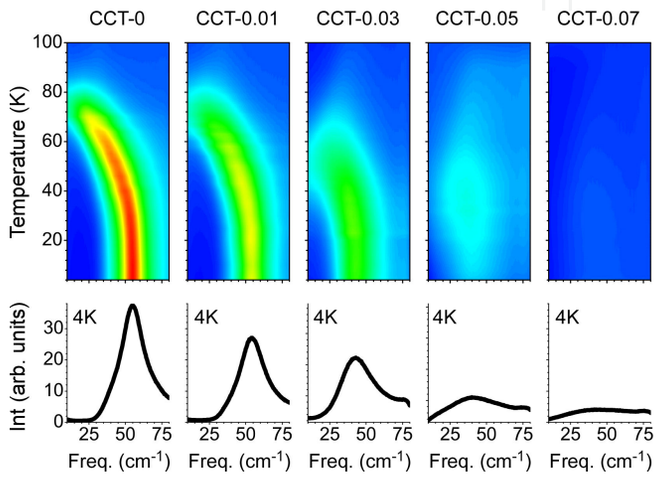

Figure 6. Contour plots for the temperature dependence of soft mode spectra in CCT-x (upper panels). Bottom panels show the low-frequency spectra observed at ~ 4 K.

Figure 7 presents the partial electronic density of states (p-DOS) for $CdTiO_3$ (left) and $CaTiO_3$ (right) obtained by the first-principles calculations, where the p-orbital of oxygen, the s-orbital of Cd and Ca, and the total DOS are denoted by oppositely hatched and blank areas, respectively. As shown in the figure, the s-orbital of Cd ion has strong hybridization with the p-orbital of oxygen. In marked contrast, the s-orbital of Ca has little hybridization, indicating larger A-O covalency in $CdTiO_3$ than $CaTiO_3$. This characteristic substantially agrees with the difference in electronegativity of Cd and Ca ions, where those in Cd and Ca are 1.7 and 1.0, respectively. A calculated charge density distributions around the O-Cd(Ca)-O bonds along the [010] direction are indicated in Fig. 8. As shown in the panels, larger charge density is observed between Cd and O ions in $CdTiO_3$, confirming its strong covalency. In contrast, Ca-O bond is nearly ionic. If the Cd(Ca) bonding is ionic, Cd(Ca) ion in the O-Cd(Ca)-O bond tends to locate a centric position. Therefore, Ca-substitution suppresses the freezing of the asymmetric stretching vibration with the off-centering of Cd(Ca) by decreasing the covalency. Since the asymmetric stretching of the O-Cd-O bond along [010] direction is suggested to be the origin of the soft mode, Ca-substitution results in the suppression of the softening of the soft mode. The present result confirms that the ferroelectric instability of CCT-x stems from A-site covalency.

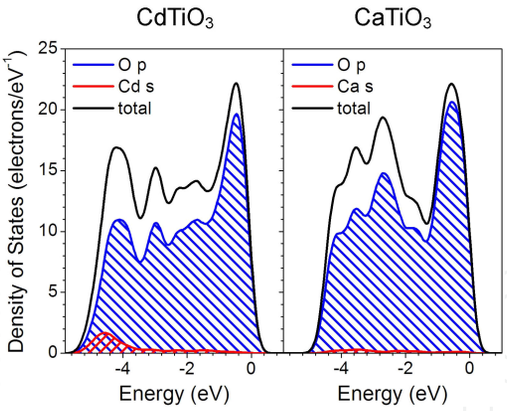

Figure 7. Partial electron density of states (p-DOS) for $CdTiO_3$ (left) and $CaTiO_3$ (right). Blue, red, and black curves represent *p* orbital of oxygen ions, *s* orbital of Cd and Ca ions, and total DOS.

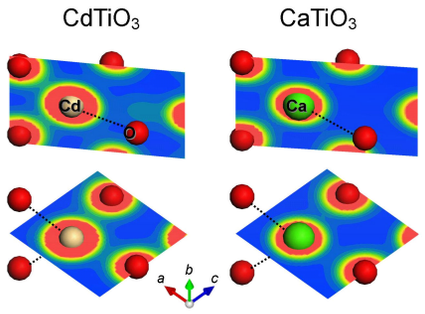

Figure 8. Cross sections of charge density around 4-coordinated Cd (left) and Ca (right) ions obtained by first principle calculations. Note that the upper and lower cross sections include O–Cd(Ca)–O bonds, which are involved in O–Cd(Ca)–O chains along the *b* and *a* direction, respectively.

4. Ferroelectric Soft Mode in the Quantum Scheme

It has been known that the quantum fluctuation plays a non-negligible role in the phase transition dynamics when the T_c goes down near 0 K, where the transition is suppressed though the dielectric permittivity reaches to several tens thousand. This effect is known as "quantum paraelectricity", which was first proposed as an origin of the giant dielectric plateau of $SrTiO_3$ at the low-temperature.[15] Twenty years later, it has been discovered that an isotope substitution with ^{18}O induces the ferroelectricity of $SrTiO_3$, attracting considerable attention of researchers.[16] In this section, the dynamics of quantum para/ferroelectric is discussed from a view point of the soft mode.

4.1. Theoretical background of the ferroelectric soft mode in the quantum scheme

In the classical case as mentioned before, the soft mode frequency can be described as Eq. 1.3. At the low-temperature, where the influence of the quantum fluctuation can not be ig-

nored, the approximation $\langle Q^2(\lambda, k)\rangle \sim k_B T$ is not appropriate. Therefore, Eq. 1.3 should be modified with quantum statistic treatment as

$$\omega_s^2 = \omega_{bare}^2(s,0) + \sum_{\lambda}\sum_{k} \frac{J(s,0;\lambda,k)}{M(s,0)} \frac{\hbar}{2M(\lambda,k)\omega(\lambda,k)} \coth\frac{\hbar\omega(\lambda,k)}{2k_B T} \tag{13}$$

At the sufficiently low-temperature, where only the Γ-point soft mode that is the optical phonon with lowest energy can be thermally excited, any other optical phonons are not effective in the second term except for $\lambda = s$ at $k = 0$. The soft mode frequency can thus be expressed as

$$\omega_s^2 = \omega_{bare}^2(s,0) + \frac{J(s,0;s,0)}{2M^2(s,0)} \frac{\hbar}{\omega_s} \coth\frac{\hbar\omega_s}{2k_B T} \tag{14}$$

As in the classical case,

$$\omega_s^2 = \omega_{bare}^2(s,0) + \frac{J(s,0;s,0)}{2M^2(s,0)} \frac{\hbar}{\omega_s} \coth\frac{\hbar\omega_s}{2k_B T_c} = 0 \tag{15}$$

gives

$$\omega_{bare}^2(s,0) = -\frac{J(s,0;s,0)}{2M^2(s,0)} \frac{\hbar}{\omega_s} \coth\frac{\hbar\omega_s}{2k_B T_c} \tag{16}$$

We thus obtain the soft mode frequency at the low-temperature,

$$\omega_s = C'\left(\frac{T_1}{2}\coth\frac{T_1}{2T} - T_c'\right)^{1/2} \tag{17}$$

with

$$C' \equiv \left[\frac{J(s,0;s,0)}{M^2(s,0)} \frac{k_B}{\omega_s^2}\right]^{1/2}, \quad T_1 \equiv \frac{\hbar\omega_s}{k_B}, \quad T_c' \equiv \frac{T_1}{2}\coth\frac{T_1}{2T_c} \tag{18}$$

In this treatment, the temperature dependence of the squared soft mode frequency, which is inversely proportional to the dielectric permittivity, in no longer linear with respect to temperature, but saturated with the constant value near 0 K. The qualitative behavior of the soft

mode in the quantum para/ferroelectrics is schematically illustrated as a function of T_1 with the fixed T'_c in Fig. 9.

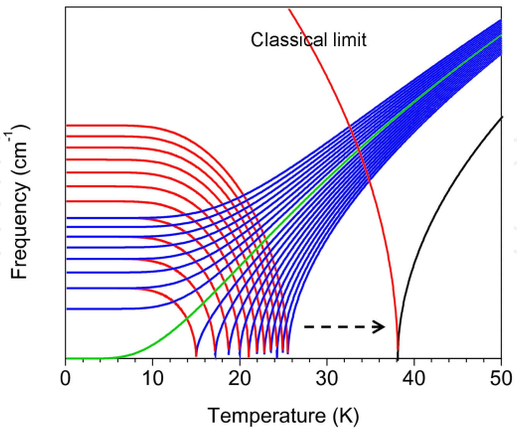

Figure 9. The schematic illustration describing the variation of the temperature dependence of the soft mode frequency as a function of T_1. See text for the detail.

The classical limit is also presented for comparison. Note that the value of T_1 is varied with constant intervals. As presented in the figure, the phase transition is completely suppressed when T_1 is sufficiently large, whereas it recovers as decreasing T_1. Interestingly, the T_1 dependence of the transition temperature becomes extremely sensitive when the transition temperature is close to 0K, suggesting that the quantum paraelectric-ferroelectric transition can be induced by subtle perturbation such as the isotope substitutions. [17]

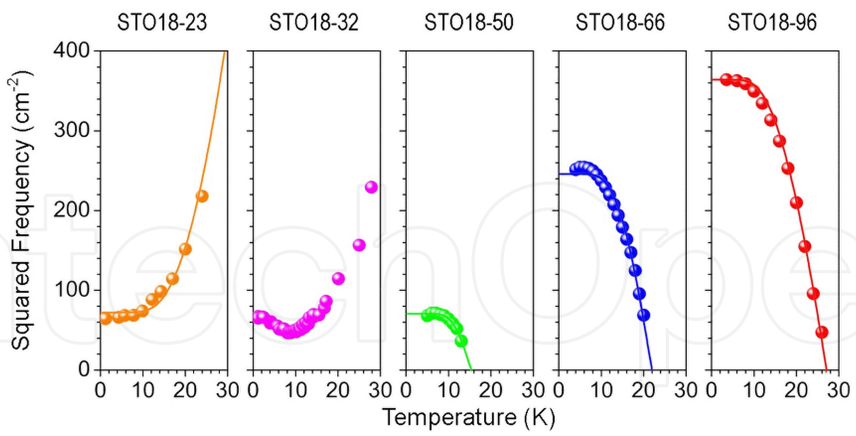

Figure 10. Temperature dependencies of the squared frequencies of the soft mode in STO18-*x* with various *x*. Solid lines in the figures denote temperature dependencies calculated by Eq. 3.7 with optimized control parameters (see text).

4.2. Experimental observation of the ferroelectric soft mode in the quantum scheme

The isotopically induced phase transition of the quantum paraelectric $SrTiO_3$ is a good example for the quantum paraelectric-ferroelectric phase transition driven by the soft mode.

http://dx.doi.org/10.5772/52059

Here we show the Raman scattering study on the soft mode in $SrTi(^{16}O_{1-x}{}^{18}O_x)_3$ (STO18-100x) as functions of temperature and the isotope substitution rate x. The experiments were performed with the Raman scattering geometries of X(YY)-X, where X, Y, and Z are denoted by the cubic coordination of $SrTiO_3$.[13,14,18]

Figure 10 presents the temperature dependence of the squared soft mode frequency in STO18-100x for 0.23, 0.32, 0.50 0.66, and 0.96, observed in the X(YY)-X scattering geometry, respectively. In x = 0.50, 0.66, and 0.96, the soft mode frequency is shown only for the ferroelectric phase. As indicated in the figure, the softening of the soft mode in STO18-23 saturates at the low-temperature region near 0 K, showing excellent agreement with the theory. Since the square of the soft mode frequency is inversely proportional to the dielectric permittivity as indicated by the LST-relation as mentioned before, it is clear that the dielectric plateau in $SrTiO_3$ stems from the soft mode dynamics. Note that the soft mode is nominally Raman inactive in the centrosymmetric structure as for the paraelectric phase of $SrTiO_3$ due to the selection rule. In the present case, however, the centrosymmetry is locally broken in the low-temperature region of STO18-100x ($x < x_c \sim 0.32$), leading to the observation of the soft mode even in the macroscopic centrosymmetry. The local non-centrosymmetric regions grow with ^{18}O-substitution to activate the soft mode spectrum even in the paraelectric phase as indicated in Fig. 11. A mechanism of such defect-induced Raman process and an expected spectral profile are discussed in detail in Ref. [13] and [14]. The date points for STO18-x ($x < x_c$) in Fig. 10 are obtained by the spectral fitting with the defect-induced Raman scattering model.

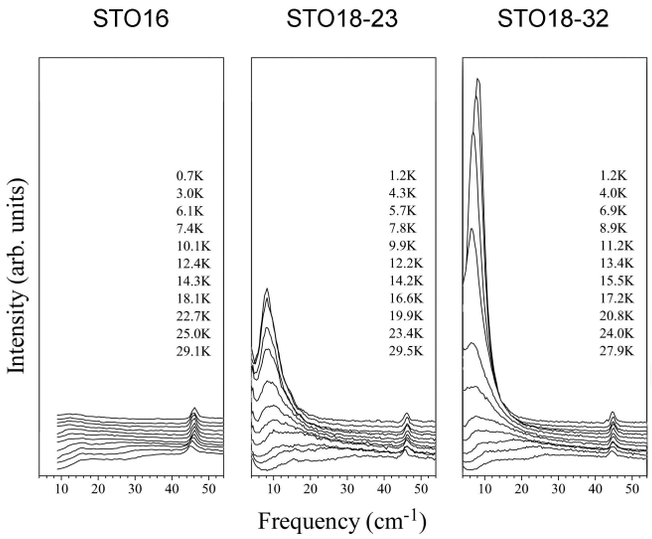

Figure 11. Temperature dependencies of the Raman spectra in STO18-x (x = 0 [STO16: the pure $SrTiO_3$], 0.23, and 0.32).

With the isotope substitution, softening of the soft mode is enhanced and the phase transition takes place above the critical concentration x_c as manifested by the hardening of the soft mode on cooling in the low temperature region. The transition temperature elevates as increasing x. The temperature dependencies of the soft modes in all samples except for that in

STO18-32 were examined by the generalized quantum Curie-Weiss law, which was proposed in Ref. 19, where the power of Eq. 3.5 is modified by γ/2;

$$\omega_s = C'\left(\frac{T_1}{2}\coth\frac{T_1}{2T} - T_c'\right)^{\gamma/2} \tag{19}$$

The γ is the one of critical exponents, which characterizes the critical behavior of the susceptibility. As seen in the figure, the plots are well reproduced by the fitting with the systematic variations of T_1 and γ as indicated in Fig. 12.

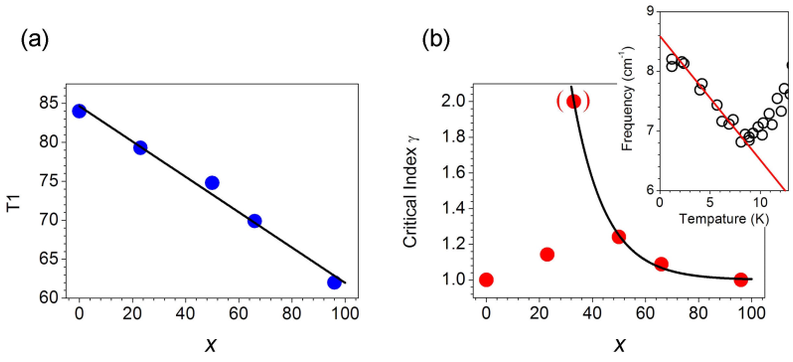

Figure 12. a) The *x* dependence of T_1obtained by the fitting. The dashed line is a guide for the eye. (b) The *x* dependence of critical exponent γ. In STO18-23, -50, -66, -96, γ is determined by the fitting of the observed soft mode frequency with Eq. 3.7. In STO18-32, we directly determined γ = 2 from the linear temperature dependence of the soft mode frequency with *T*, as seen in the inset. The solid lines are eye guides.

In STO18-32, the strongly rounded soft mode behavior keeps us from fitting with Eq. 3.7. However, we can determine γ = 2 for STO18-32 from the obvious linear temperature dependence of the soft mode frequency, as seen in the inset of the panel (b). It should be noted here that γ = 2 corresponds to the theoretical value for the quantum ferroelectric phase transition [20–22], and is caused by the quantum mechanical noncommutativity between kinetic and potential energy. These results show experimentally that the quantum phase transition of STO18-*x* is an ideal soft mode-type transition driven by direct control of the quantum fluctuation with the ^{18}O-substitution. An origin of the strongly rounded softening was suggested in our previous study to be the nanoscopic phase coexistence between ferroelectric and paraelectric region. (See Ref. 18 for the detail)

5. Summary

In the present review, we overviewed the soft mode behavior in both classical and quantum schemes through Raman scattering experiment in the $CdTiO_3$ and the ^{18}O-substituted $SrTiO_3$. The analyses show excellent agreement qualitatively between the fundamental theory and experimental observations. The systematic studies with Raman scattering experi-

ments and the first-principles calculations on Ca-substituted $CdTiO_3$ clarified that the covalency between constituent cation and oxygen plays an essential role in the origin of the soft mode. We hope the present review serves better understanding on the mechanism of displacive-type ferroelectric phase transition.

Author details

Hiroki Taniguchi[1*], Hiroki Moriwake[2], Toshirou Yagi[3] and Mitsuru Itoh[1]

*Address all correspondence to:

1 Materials and Science Laboratory, Tokyo Institute of Technology, Yokohama, Japan

2 Nanostructures Research Laboratory, Japan Fine Ceramics Center, Nagoya, Japan

3 Research Institute for Electronic Science, Hokkaido University, Sapporo, Japan

References

[1] Line, M. E., & Glass, A. M. (1997). Principles and Applications of Ferroelectrics and Related Materials,. Claredon, Oxford,.

[2] Cochran, W. (1960). Crystal stability and the theory of ferroelectricity. *Adv. Phys.*, 9, 387.

[3] Cochran, W. (1961). Crystal stability and the theory of ferroelectricity part II. Piezoelectric crystals. *Adv. Phys.*, 10, 401 EOF-420 EOF.

[4] Scott, J. F. (1974). Soft-mode spectroscopy: Experimental studies of structural phase transitions. Rev. Mod. Phys. ., 46, 83 EOF-128 EOF.

[5] Shan, Y. J., Mori, H., Imoto, H., & Itoh, M. (2002). Ferroelectric Phase Transition in Perovskite Oxide $CdTiO_3$. *Ferroelectrics*, 381 EOF-386 EOF.

[6] Shan, Y. J., Mori, H., Tezuka, K., Imoto, H., & Itoh, M. (2003). Ferroelectric Phase Transition in $CdTiO_3$ Single Crystal. *Ferroelectrics*, 107 EOF-112 EOF.

[7] Moriwake, H., Kuwabara, A., Fisher, C. A. J., Taniguchi, H., Itoh, M., & Tanaka, I. (2011). First-principles calculations of lattice dynamics in $CdTiO_3$ and $CaTiO_3$: Phase stability and ferroelectricity. *Phys. Rev. B*, 84, 104.

[8] Taniguchi, H., Shan, Y. J., Mori, H., & Itoh, M. (2007). Critical soft-mode dynamics and unusual anticrossing in $CdTiO_3$ studied by Raman scattering. *Phys. Rev. B*, 76, 212103.

[9] Clark, S. J., Segall, M. D., Pickard, C. J., Hasnip, P. J., Probert, M. I. J., Refson, K., & Payne, M. C. (2005). First principles methods using CASTEP. *Z. Kristallogr*, 220, 567.

[10] Bersuker, I. B. (1995). Recent development of the vibronic theory of ferroelectricity:. *Ferroelectrics*, 164, 75.

[11] Taniguchi, H., Soon, H. P., Shimizu, T., Moriwake, H., Shan, Y. J., & Itoh, M. (2011). Mechanism for suppression of ferroelectricity in $Cd_{1-x}Ca_xTiO_3$. *Phys. Rev. B*, 84, 174106.

[12] Taniguchi, H., Soon, H. P., Moriwake, H., Shan, Y. J., & Itoh, M. (2012). Effect of Ca-Substitution on $CdTiO_3$ Studied by Raman Scattering and First Principles Calculations. *Ferroelectrics*, 268 EOF-273 EOF.

[13] Taniguchi, H., Takesada, M., Itoh, M., & Yagi, T. (2004). Effect of oxygen isotope exchange on ferroelectric microregion in $SrTiO_3$ studied by Raman scattering. *J. Phys. Soc. Jpn.*, 73, 3262 EOF-3265 EOF.

[14] Taniguchi, H., Takesada, M., Itoh, M., & Yagi, T. (2005). Isotope effect on the soft-mode dynamics of $SrTiO_3$ studied by Raman scattering. *Phys. Rev. B*, 72, 064111.

[15] Müller, K. A., Burkard, H., & Sr Ti, O. (1979). An intrinsic quantum paraelectric below 4 K. *Phys. Rev. B*, 19, 3593.

[16] Itoh, M., Wang, R., Inaguma, Y., Yamaguchi, Y., Shan, Y. J., & Nakamura, T. (1999). Ferroelectricity Induced by Oxygen Isotope Exchange in Strontium Titanate Perovskite. *Phys. Rev. Lett.*, 82, 3540 EOF-3543 EOF.

[17] Tokunaga, M., & Aikawa, Y. (2010). Isotope-Induced Ferroelectric Phase Transition in Strontium Titanate Only by a Decrease in Zero-Point Vibration Frequency. *J. Phys. Soc. Jpn.*, 79, 024707.

[18] Taniguchi, H., Itoh, M., & Yagi, T. (2007). Ideal Soft Mode-Type Quantum Phase Transition and Phase Coexistence at Quantum Critical Point in ^{18}O-Exchanged $SrTiO_3$. *Phys. Rev. Lett.*, 99, 017602 EOF.

[19] Dec, J., & Kleemann, W. (1998). From barrett to generalized quantum curie-weiss law. *Solid State Commun.*, 106, 695 EOF.

[20] Vojta, M. (2003). Quantum phase transitions. *Rep. Prog. Phys.*, 66, 2069.

[21] Sondhi, S. L., Girvin, S. M., Carini, J. P., & Shahar, D. (1997). Continuous quantum phase transitions. *Rev. Mod. Phys.*, 69, 315 EOF-333 EOF.

[22] Schneider, T., & Stoll, E. F. (1976). Quantum effects in an n-component vector model for structural phase transitions. *Phys. Rev. B*, 13, 1123 EOF-1130 EOF.